

## ORIGINAL ARTICLE

## Study of Cross-Combination and Square-Combination Configuration Magnetic Field on Tungsten Inert Gas Welding

A.S. Baskoro, M.A. Amat and B. Arisoni

Department of Mechanical Engineering, Faculty of Engineering, Universitas Indonesia, 16424 Depok Indonesia  
Phone: +62-21-7270032; Fax: +62-21-7270032

**ABSTRACT** – In this study, cross-combination and square-combination configuration of the permanent external magnet were used in tungsten inert gas welding process. The external magnetic field effect to the arc plasma was observed using two cameras from the front view and side view. The depth of penetration and weld profile was investigated after welding. In this study, two types of magnets were employed; a 3 mm magnet with intensity ranging from 270-280 mT and a 5 mm magnet with 400-415 mT. Each configuration has three sub-configurations: forward, backward, and side, so there were 12 parameters in this study. The result shows that a cross-combination 5 mm magnet can increase weld penetration in any position, forward, backward or side deflection, and improve the depth-to-width ratio, however using 3 mm magnet did not influence the penetration significantly. Cross-combination has more stiffness and stability of the arc than square-combination. Most configurations have the same size weld bead width. Square combinations had fluctuated result, stiffness and stability of the arc was poor. This investigation aims to enlarge our understanding of the magnetic field effect on the arc plasma and the weld profile. In future, the arc blow effect from the external magnetic field can be controlled and regulated to improve TIG welding performance.

**ARTICLE HISTORY**Received: 12<sup>th</sup> Jan 2021Revised: 23<sup>rd</sup> Mar 2021Accepted: 4<sup>th</sup> June 2021**KEYWORDS**

TIG;

Permanent magnet;

Arc blow;

Arc image;

Weld penetration

### INTRODUCTION

Gas tungsten arc welding (GTAW) or tungsten inert gas (TIG) Welding have been widely used in the manufacturing industry, such as the automobile industry and other transportation industry [1-2]. TIG welding is commonly used when precision and high quality are required [3]. The research and development related to TIG welding improve the welding process's effectiveness and performance and improve the energy efficiency in recent years is vital because of the global warming issue [4]. Due to the free arc, when TIG welding is in low-level current applied, the energy density and the arc pressure are relatively poor, which leads to shallower melting depth. In order to increase the melting depth, lowering welding speed is a common solution. However, low welding speed increases exposed annealing time and reduced the welding efficiency. The annealing time effect is problematic; the more exposure time from the heating effect, it tends to deeper reduced strength in the HAZ region. Another common solution to increase welding efficiency is using a high-level current and faster welding speed. However, it also has a problematic problem. High-level current tends to damage the tungsten tip shape progressively, resulting in an unbalance arc shape, which sometimes can lead to improper welding and defects.

Research in TIG welding related to applying the electromagnetic field (EMF) with induction coil or permanent magnet has grown in recent years. However, research related to EMF in gas metal arc welding (GMAW) or GTAW has been introduced for a long time since 1962 by Brown et al. [5]. The technology used EMF with an induction coil or magnetic field from a permanent magnet is used for some reasons, such as associated with modifying the microstructure [6-10], improving corrosion resistance and pitting resistance [8, 11-13], enhanced weld penetration and the characteristics [14, 15], the stability of the arc plasma [16-18], controlling the droplet transfer [8, 19], improving the joint strength [9], and fatigue damage [10]. Compared to the traditional or conventional TIG welding, TIG assisted with an external permanent magnet can improve the depth-to-width ratio and reduce the corresponding heat input. Zhu et al. [6] implement external constant magnetic field in hybrid laser-GMAW. The EMF resulting in a better arc shape and droplet transfer. Overall increases the quality of the weld joint. Liu et al. [7] propose the lap shear joint AZ31 and AA6061 using TIG assisted with three types of magnetic pole's configuration using magnetic oscillation system. They found that the oscillation system tends to decrease the welding penetration and increase welding width, and it is suitable for the lap-shear joint because the wetting behaviour of molten improved. Zhao et al. [8] improved atmospheric corrosion resistance using assisted traverse magnetic field in high-speed HW-TIG (hot wire). Chen et al. [9] improve pitting corrosion resistance in stainless steel using a constant magnetic field below the workpiece in hybrid laser-TIG. The EMF produce the stirring effect mechanism that leads to a decrease in the diversity of the thermal gradients. While Curiel et al. [13] earlier had applied the same strategy in SS304 to improve pitting and intergranular corrosion. Rosado-Carrasco et al. [10] improved

fatigue damage resistance by applying external axial current EMF in duplex stainless steel using GMAW. Shang Liu et al. [14] applied cusp magnetic field (CMF) in K-TIG welding. The CMF has shown a better constrain effect compared to the non-CMF. The melting zone size decrease, the depth and arc voltage increase. The pole's angle is the crucial factor in the CMF result.

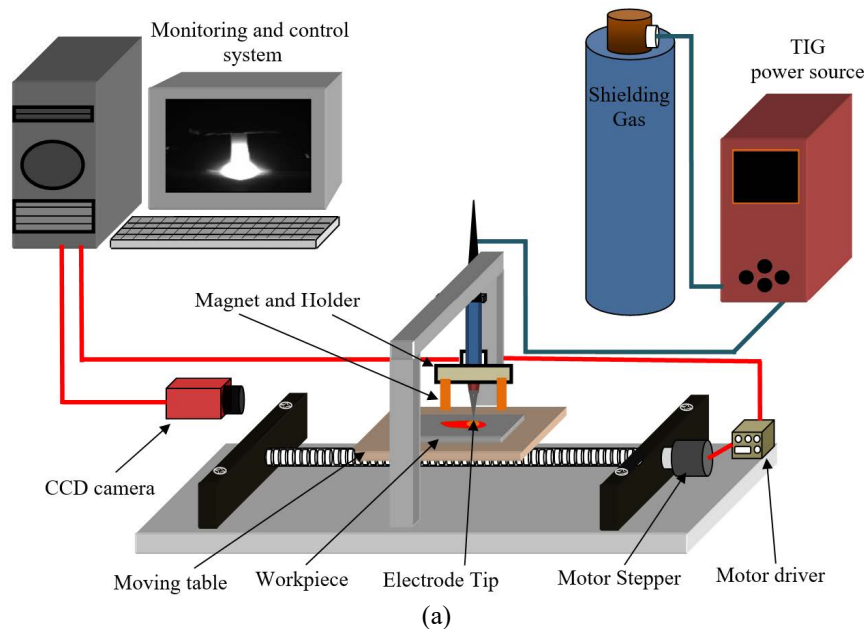
In general, EMF leads to unbalanced arc stability resulting in improper and unwanted weld profile. In many cases, it is totally avoided or sometimes controlling to reducing the amount of unwanted EMF on the welding process and improving the quality of welding [20]. In recent years, several studies were conducted to apply EMF to control the arc plasma deflection. It was using the proper configuration so that the vector of the magnetic field can enhance the penetration. In this study, several permanent magnets NdFeB configurations were proposed in a new design holder that can be attached directly to TIG ceramic cup. The purpose of this study is to validate the prediction of the arc blow with the experimental result and then investigate whether the proposed configurations had a good result in weld profile and weld penetration.

## MATERIALS AND METHOD

The materials used in this study were SS304 with a thickness of 5 mm. The specimens were cut into a dimension of 150×50×5 mm, while the welding process used Miller Dynasty 210 DX pulse welding machine. A high-speed camera Guppy pro, and a mobile phone camera were used to monitor the arc shape from the front view and the side view. Figure 1 schematically shows the experimental setup of the TIG welding apparatus. The external magnetic field was generated by rectangular NdFeB permanent magnets with 30×10×3 mm and 30×10×5 mm. The magnetic induction intensity of each magnet is measured with a gaussmeter. Table 1 shows the magnitude of the intensity. The measured strength magnetic fields are the inputs for the simulation. The configuration of the magnetic poles was classified into two types; cross combination and square combination, as shown in Figure 2. All configurations were perpendicular to the workpiece. The square combination was similar to the cusp magnetic field configuration (CMF) [5] but with different combination poles. CMF had pole's configuration of N-S-N-S, while this experiment is using configuration N-N-S-S. Each configuration has three sub configurations, which are forward, backward, and side.

**Table 1.** Composition of magnet strength (mT).

No. magnet	3 mm				5 mm			
	1	2	3	4	1	2	3	4
N	280	274	272	283	418	415	401	412
S	273	275	270	273	413	416	416	411
Avg.	276.5	274.5	271.5	278	415.5	415.5	408.5	411.5



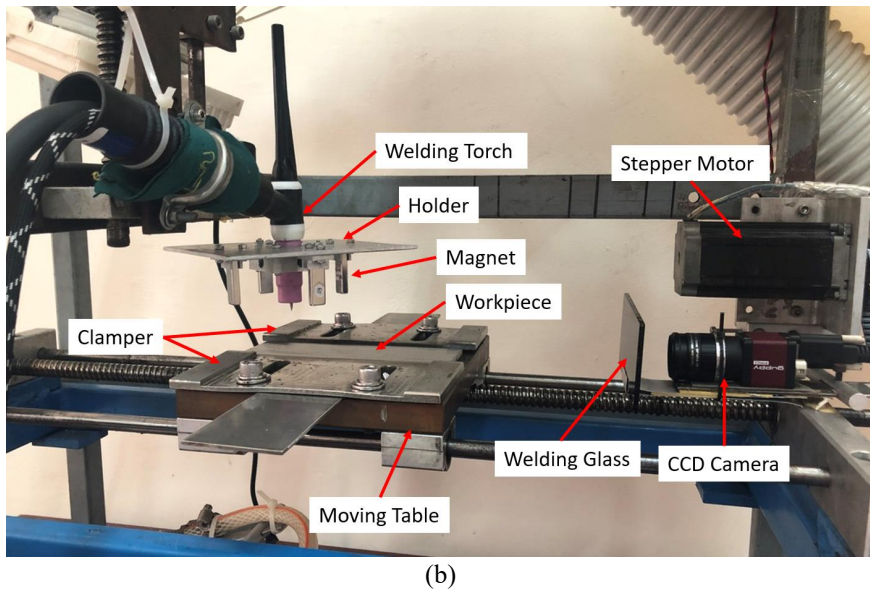


Figure 1. (a) Schematic illustration and (b) photograph of experimental apparatus.

DC polarity was employed in the welding process. At the initial welding process, holding time or pre-heating time was not given. High purity argon was used as a shielding gas with a flow rate of 10 L/min at the top side welded pool. The tungsten electrode was set perpendicular to the workpiece with a distance of 3 mm (Table 2). Macrostructure observation, depth measurement, and top bead width measurement were conducted using DINO-LITE. The specimens were prepared using meshing and polishing tools and etched using picric acid to reveal macrograph then measured the depth. Statistical methods were used to analyse the magnet’s configurations and strength on the weld penetration and size of the weld bead. Arc image confirms the hypothetical shape that was analysed and predicted from the simulation magnetic field using free software Vizimag.

Table 2. Welding process parameters.

Parameter	Specification
Polarity	DC
Weld current (A)	100
Welding speed (mm/s)	2
Electrode	EWCe-2 (Ø 2.4 mm)
Tungsten distance to material (mm)	3
Shielding gas	Pure argon (99.9%)
Top side shielding gas flow rate (l/min)	10

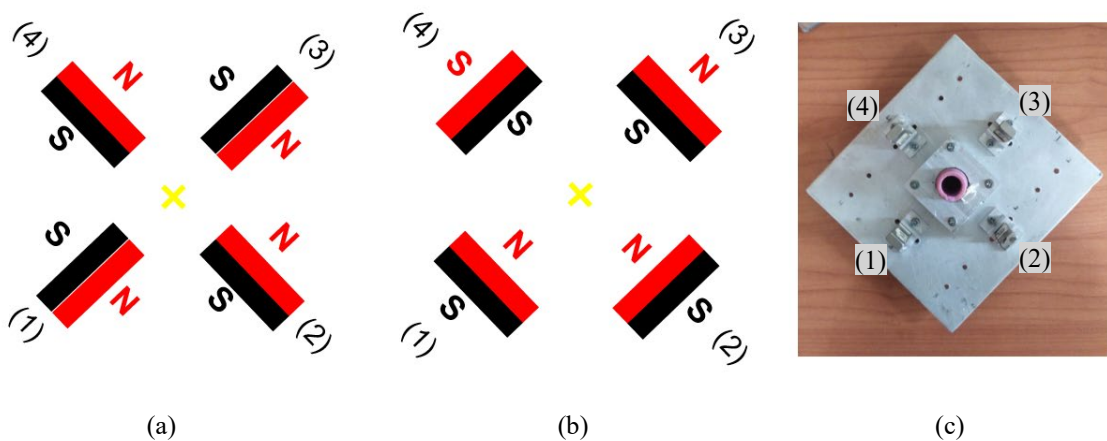


Figure 2. (a) Cross-combination and (b), (c) square-combination arrangement.

### SIMULATION AND ARC SHAPE PREDICTION

The model is based on the permanent magnet experimental model’s configuration to establish the magnetic field’s direction and distribution, and with magnitude, a simple 2D Finite Element Difference model is applied. Many researchers have conducted complex 3D model of arc and weld pool [17, 21-25]. The complicated coupling model and mathematical conservation model into the software make it hard to tasking in early presumable research. Therefore, the simple approach

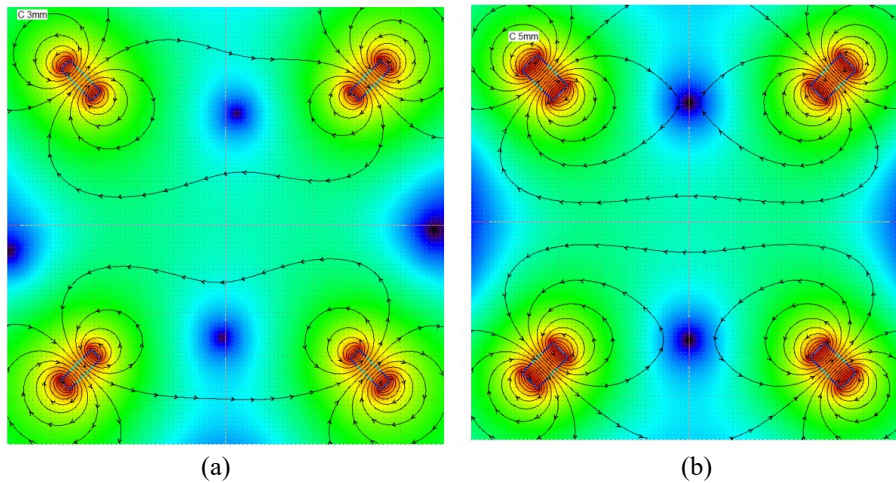
is affordable for this research until the investigation is deeper to understand current density, electric potential, pressure distribution, velocity distribution, and temperature distribution. This simpler way approach considers the influence of the external magnetic field that could generate the Lorentz force and change the arc weld's shape. The simulation is solved by using Vizimag 3.18 software, and the model is built in 2D-Cartesian coordinate. The following assumptions were given:

- i. Homogeneous condition, uniform permeability of neodymium magnet is  $\mu = 1.1$
- ii. No external source, except the permanent magnet,  $\partial B/\partial t = 0$  (magnetostatic case)
- iii. 3<sup>rd</sup> dimension is neglected
- iv. The arc prediction curve was made by the right-hand rule of Lorentz equation

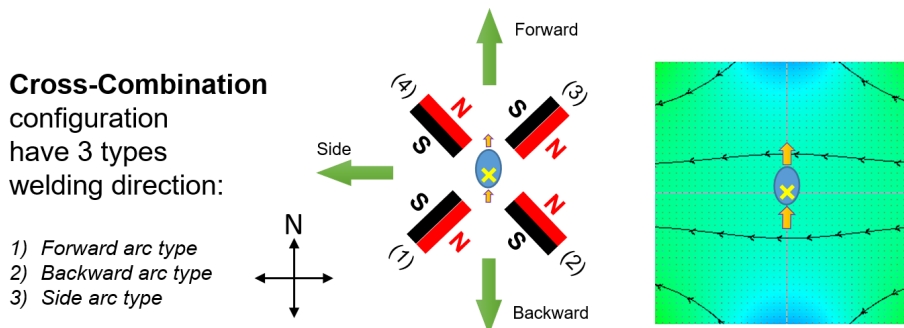
## RESULTS AND DISCUSSION

### Simulations and Predictions

Figure 3 shows magnetic field contour from the cross-combination configuration of 3 mm and 5 mm in thickness. Figure 4 shows the arc blow prediction was made by the right-hand rule without any calculation to measure the magnitude. By reviewing the contour and the magnetic field vector with the current flow through in the plane (or paper) as shown in the yellow cross mark, the right-hand rule results from Lorentz force going up (north side). The arc was deflected in the same direction as the Lorentz force did. The green arrow sign was a welding direction. There were three welding directions, named forward deflection, backward deflection, and side deflection. It was named based on the arc blow deflected relative to the welding direction, such as forward, the arc blow deflected to the north side, and the welding direction going to the north. Figure 5 shows magnetic field contour and arc blow prediction results by the square-combination configuration of 3 mm and 5 mm in thickness. The colour contour in the square-combination shows darker blue, while cross-combination shows lighter blue in the centre arc welding. Darker blue means lesser magnitude, hence cross-combination having a bigger magnitude of magnetic field compared to the square combination.



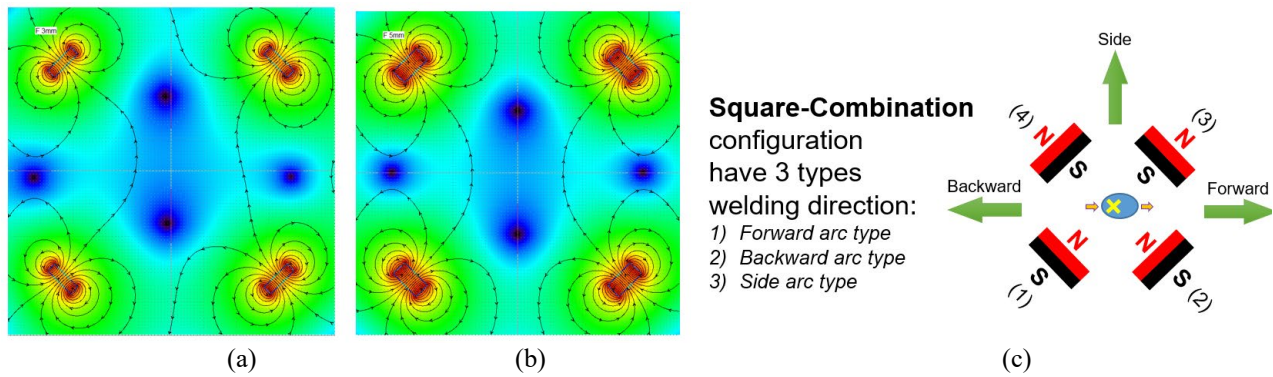
**Figure 3.** Magnetic field contour cross-combination configuration for (a) 3 mm and (b) 5 mm thickness.



**Figure 4.** The arc blow prediction of cross-combination configuration.

The square-combination configuration in Figure 5 was similar to the configuration proposed by Nomura et al. [26, 27]. The difference was in the sequence pole. Nomura et al. used the N-S-N-S combination, while this study used N-N-S-S or S-S-N-N combination configuration. Based upon the configuration category made by Wu et al. [5], cross-combination configuration can be categorised into cups-magnetic-field (CMF). However, the pole's face cross-combination was rotated 90°; hence it was perpendicular to the arc. Nomura's result [26] showed that the arc shape

changed to elliptical form and also increasing the depth-to-width ratio slightly. They showed applied CMF can have potential in high-speed welding.



**Figure 5.** Magnetic field contour square-combination configuration of (a) 3 mm, (b) 5 mm (mid) and (c) the arc blow prediction.

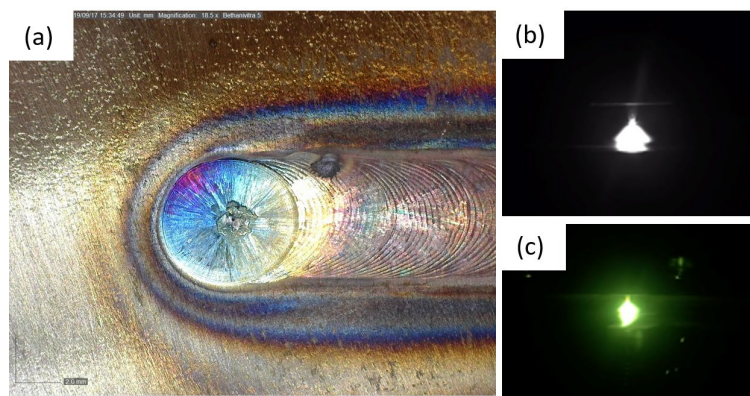
The other work by Nomura [27] proposed CMF with a different configuration pole. The first one was called horizontal position, while his second study used vertical position. The result showed the vertical magnet had a more substantial effect compared to the horizontal magnet. Table 3 shows the magnitude of magnetic field simulation and validation before the experiment. The strength of the simulation was measured in a 3 mm radius from the centre of the arc weld; therefore, the results were varied in range scale. This was performed to compensate for the validation measurement. Validation measurement measured the intensity in the same point location (x, y, z), the centre of the arc weld. The sensor was placed between the electrode and the workpiece. To compensate for human error because of misplaced (about ±1mm), the simulation was measured in a 3 mm radius. Table 3 shows cross-combination has higher magnetic field intensity compared to square-combination. The cross configuration with 5 mm is three times bigger than the cross 3 mm, while the square with 5 mm is two times bigger than the square configuration with 3 mm.

**Table 3.** Magnetic field magnitude simulation and experiment.

Configuration	Simulation	Validation
Cross (3mm)	1.93-1.96 mT	1.95 mT
Cross (5mm)	5.93-6.02 mT	5.97 mT
Square (3mm)	1.05-1.15 mT	1.11 mT
Square (5mm)	2.36-2.47 mT	2.41 mT

**Arc Blow Image Comparison**

Figure 6 shows the non-magnet weldment results. In Figure 6(a), the end welded mark have a perfect circle, while Figure 6(b) and 6(c) shows the axisymmetric plasma arc. Figure 7 shows the arc image and end weld mark from cross and square configuration. Forward deflection and backward deflection can be seen from the side camera, while side deflection can be seen from the front camera. The comparison made with Nomura works [26, 27] showed that the N-N-S-S configuration has a different result in changing the arc blow effect. The arc blow results were consistent with the work showed by Baskoro et al. [15] with the same type configuration N-N-S-S. Their literature proposed many different configurations in a vertical position, namely perpendicular (PP-NNSS) and horizontal position, namely parallel (PR-NNSS).



**Figure 6.** Non-magnet result: (a) end weld mark, (b) arc weld from front camera view, (c) arc weld from side camera view.

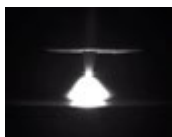
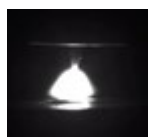
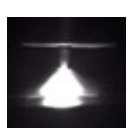


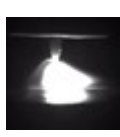
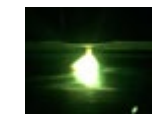


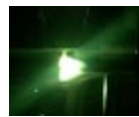
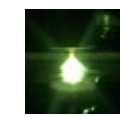
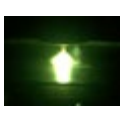
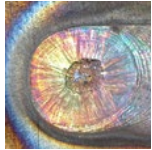



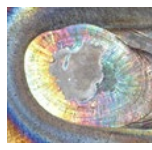









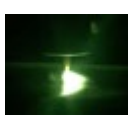

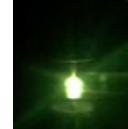

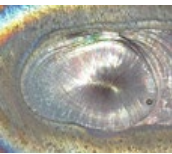

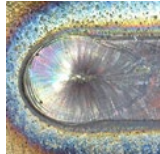
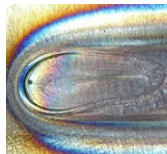
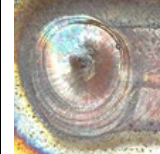

	Forward		Backward		Side	
	Cross	Square	Cross	Square	Cross	Square
Front camera (3 mm)						
Side camera (3 mm)						
End welded mark (3 mm)						
Front camera (5 mm)						
Side camera (5 mm)						
End welded mark (5 mm)						

Figure 7. Arc image and end weld mark from different sub configurations.

Figure 8 shows the front camera view of the side deflection. It is clearly shown that square-combination has a higher deflected arc with less pressurisation arc to the workpiece. Hence the arc blow tends to go further and longer compared to the cross-combination configuration. The end welded mark shows proof; even cross-combination has a higher magnetic intensity than the square-combination (see Table 3). The arc blow seems to have less blow, and the end welded mark has slightly elliptical. The end welded mark of square-combination has a strong elliptical shape.

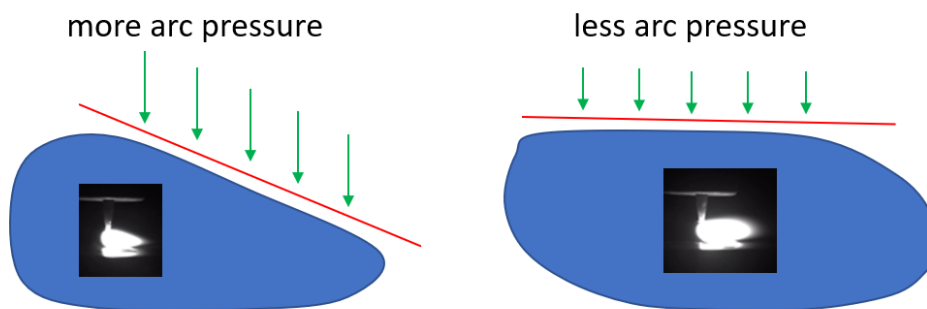


Figure 8. Hypothetical analysis of arc pressure between (a) cross-combination and (b) square-combination.

**Weld Penetration and Bead Width Comparison**

To measure the bead width, eight points were taken with a distance of 1 cm from each point. The welding’s starting point is given a value of 0 cm with an end value of 9 or 10 cm. The measured points were taken at 1 cm to 8 cm for each configuration and calculated for mean and standard deviation. After measurement, specimens were cut into three parts with a distance of 25%, 50%, and 75% of the total welding length. Each part cutting specimen was meshed, polished, and etched with picric acid to reveal the macrograph. Then the depth for 3 section parts was measured. After being measured, the means and standard deviation were calculated then. For simplification, the cross-combination forward, backward, and

side deflection will be named CF, CB, and CS. And for square-combination, it will be named as SF, SB, and SS, respectively.

The magnet configurations were compared to the non-magnet result using the two-tail test statistical test if both were the same or different. As shown in Figure 9(a), the depth penetration comparison test using statistical test shows for 3 mm magnets, CF, CB, CS, and SS, have similar results with the non-magnet. At the same time, SF tends to increase but less significant, and SB decreases significantly. For 5 mm magnets, CF, CB, and CS increase significantly, especially CB, almost 80% deeper than non-magnet. The different results are shown by the square configuration where the results are quite fluctuating; SF has similar results to non-magnet with SB decreases and SS increases. However, the SS increases and have a high deviation, which means the penetration depth fluctuates over the weldment. Figure 9(b) shows the weld bead width where almost all configurations resulted less than or equal to non-magnet. Only SS 5 mm results in a significant increase in width, increasing up to 55% compared to the non-magnet. The others configuration for 3 mm, CF, CS, SB, SS, and CS-5mm show a similar result to non-magnet. While the 3 mm CB and SF, 5 mm CF, CB, SF, and SB have a smaller width than non-magnet. The bead with result in this study much more obvious and consistent with the result from previous research by Baskoro et al. [15]. However, Baskoro et al. did not include the macrograph to measure the depth. Instead, they calculated the depth using projection from top bead width and back bead width.

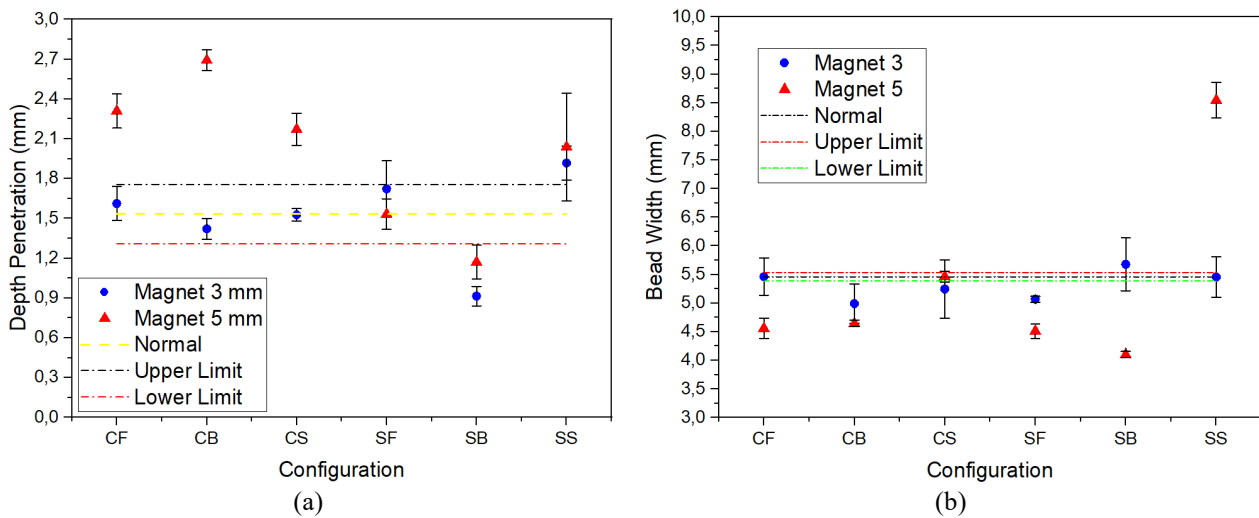


Figure 9. (a) Depth penetration and (b) bead width of different configurations.

Increasing magnet intensity almost three times has a significant result in cross-combination configuration. In contrast, in square-combination configuration, SF and SS have similar results to non-magnet, and SB slightly increases, even though the magnetic intensity increases more than two times (see Table 3). CB and SB comparison shows an inverse effect on the implementation of the permanent magnet. CB tends to go deeper, while SB tends to decrease the penetration. It is confirmed that square-combination has a negative arc pressure making the total pressure is less than the normal pressure (non-magnet pressure). At the same time, CB shows the other way has positive arc pressure making the total pressure more than the normal pressure. As a result, cross-combination has more stability and stiffness than square-combination. CF and CB bead width decreased; it is shown that the produced arc was slimmer compared to non-magnet, hence tends to have higher current density and has higher energy density. This result is very much in line with the result of higher current density having deeper penetration for CF and CB. The forward deflection has a pre-heating arc, while the backward deflection has a post-heating arc. In the CF and CB case, the post-heating method (CB) wins slightly deeper in penetration than the pre-heating method (CF). Meanwhile, side deflection has not given any advantages to any heating method, so it has the smallest value among the three (CF, CB, CS). With the increase in penetration and reduction in bead width, the cross-combination significantly improves the depth-to-width ratio. Figure 10 shows the illustration comparison of arc shape of CB, CF, and CS to non-magnet. Figure 11 shows the one from three cross-sections of the weld specimen and the top view of the weld bead.

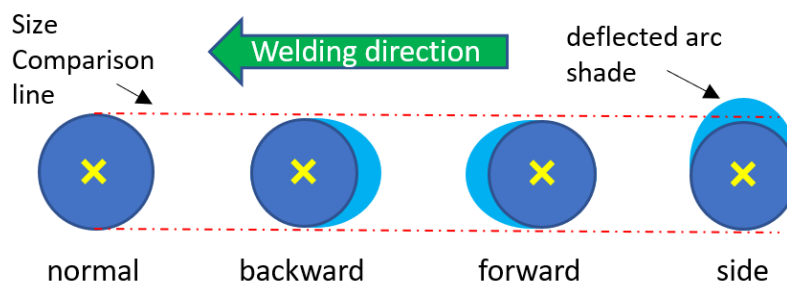


Figure 10. Illustration of the arc shape of CB, CF and CS to non-magnet.

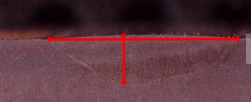

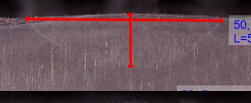
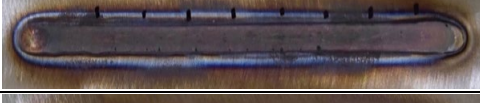


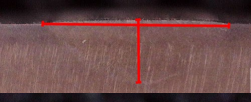

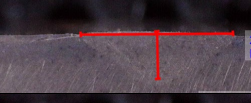

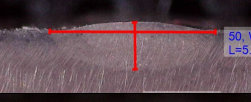



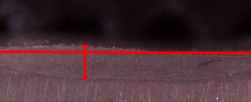

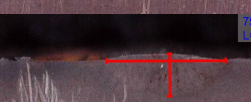
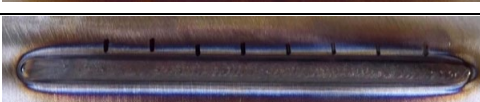
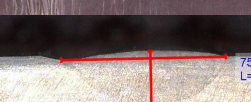



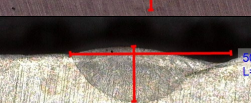

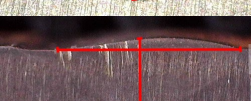

Configuration		Depth penetration	Weld bead width
Non-magnet			
Forward	Cross 3 mm		
	Cross 5 mm		
	Square 3 mm		
	Square 5 mm		
Backward	Cross 3 mm		
	Cross 5 mm		
	Square 3 mm		
	Square 5 mm		
Side	Cross 3 mm		
	Cross 5 mm		
	Square 3 mm		
	Square 5 mm		

Figure 11. Cross-section and top view of weld specimens.

### CONCLUSION

The conclusions can be drawn as follows:

- i. The magnetic field strength from real measurement is close to the simulation value. Lorentz force and arc prediction correspond to the experiment results in all configurations.
- ii. The cross-combination has more stiffness and stability of the arc than square-combination; thus, square-combination has a higher deflected arc. The cross combinations 5 mm have deeper penetration, while 3 mm do not influence the penetration. Almost all configurations have less than or equal to the non-magnet in terms of weld bead width.
- iii. The cross 5 mm has a smaller bead width and deeper penetration; hence, it has higher current density and energy density and significantly improves the depth-to-width ratio. The square combinations have fluctuated result and need further investigation.



## ACKNOWLEDGEMENT

The authors would like to express their sincere gratitude for the financial support from PDUPT Kemenristek/BRIN 2020 with contract number NKB-2836/UN2.RST/HKP.05.00/2020.

## REFERENCES

- [1] Widyianto A, Baskoro AS, Kiswanto G. Effect of pulse currents on weld geometry and angular distortion in pulsed GTAW of 304 stainless steel butt joint. *International Journal of Automotive and Mechanical Engineering* 2020; 17(1): 7687-7694.
- [2] Baskoro AS, Milyardi I, Amat MA. The effect of welding parameter on mechanical properties and macrostructure of AA1100 using autogenous TIG welding. *International Journal of Automotive and Mechanical Engineering* 2020; 17(1): 7562-7569.
- [3] Shankar MCG, Jayashree PK, Sharma SS, et al. Quality enhancement of TIG welded Al6061 SiCp composites by age hardening process. *International Journal of Automotive and Mechanical Engineering* 2018; 15(3): 5573-5582.
- [4] Yalew SG, van Vliet MTH, Gernaat DEHJ, et al. Impacts of climate change on energy systems in global and regional scenarios. *Nature Energy* 2020; 5(10): 794-802.
- [5] Wu H, Chang Y, Lu L, Bai J. Review on magnetically controlled arc welding process. *International Journal of Advanced Manufacturing Technology* 2017; 91(9-12): 4263-4273.
- [6] Zhu Z, Ma X, Wang C, et al. effect of microstructure and microtexture modified by magnetic field on as-weld notch bending performance. *Journal of Materials Processing Technology* 2021; 289: 116958.
- [7] Liu YB, Li JZ, Sun QJ, et al. Optimisation of magnetic oscillation system and microstructural characteristics in arc welding of Al/Mg alloys. *Journal of Manufacturing Processes* 2019; 39: 69-78.
- [8] Zhao M, Chen J, Yu M, et al. effect of transverse magnetic field on weld formation and microstructure & properties of high-speed hot-wire tungsten inert gas welding joints. *Science and Technology of Welding and Joining* 2020; 25(5): 407-414.
- [9] Chen R, Jiang P, Shao X, et al. Effect of static magnetic field on microstructures and mechanical properties of laser-MIG hybrid welding for 304 stainless steel. *The International Journal of Advanced Manufacturing Technology* 2017; 91(9): 3437-3447.
- [10] Rosado-Carrasco J, Krupp U, López-Morelos VH, et al. effect of a magnetic field applied during fusion welding on the fatigue damage of 2205 duplex stainless steel joints. *International Journal of Fatigue* 2019; 121: 243-251.
- [11] Chen R, Jiang P, Shao X, et al. Effect of magnetic field applied during laser-arc hybrid welding in improving the pitting resistance of the welded zone in austenitic stainless steel. *Corrosion Science* 2017; 126: 385-391.
- [12] Wu D, Hu C, Zhao W, et al. Influence of external magnetic field on twin-wire indirect arc surfacing stainless steel layer. *Vacuum* 2019; 169: 108958.
- [13] Curiel FF, García R, López VH, González-Sánchez J. Effect of magnetic field applied during gas metal arc welding on the resistance to localised corrosion of the heat affected zone in AISI 304 stainless steel. *Corrosion Science* 2011; 53(7): 2393-2399.
- [14] Liu S, Liu ZM, Zhao XC, Fan XG. Influence of cusp magnetic field configuration on K-TIG welding arc penetration behavior. *Journal of Manufacturing Processes* 2020; 53: 229-237.
- [15] Baskoro AS, Fauzian A, Basalamah H, et al. Improving weld penetration by employing of magnetic poles' configurations to an autogenous tungsten inert gas (TIG) welding. *The International Journal of Advanced Manufacturing Technology* 2018; 99(5): 1603-1613.
- [16] Chen Q, Chen J, Lu S, et al. Study of high-speed GMAW assisted by compound external magnetic field. *Welding in the World* 2020; 64(5): 885-901.
- [17] Wang L, Chen J, Jiang C, Wu C. Numerical simulations of arc plasma under external magnetic field-assisted gas metal arc welding. *AIP Advances* 2020; 10(6).
- [18] Wu H, Chang Y, Mei Q, Liu D. Research advances in high-energy TIG arc welding. *International Journal of Advanced Manufacturing Technology* 2019; 104(1-4): 391-410.
- [19] Voigt AL, Cunha TVD, Niño CE. Conception, implementation and evaluation of induction wire heating system applied to hot wire GTAW (IHW-GTAW). *Journal of Materials Processing Technology* 2020; 281: 116615.
- [20] Jones RB. New system to control magnetic arc blow in welding. *Journal of Ship Production* 1995; 11(1): 30-33.
- [21] Chen T, Xiaoning Z, Bai B, et al. Numerical study of DC argon arc with axial magnetic fields. *Plasma Chemistry and Plasma Processing* 2015; 35(1): 61-74.
- [22] Yin X, Gou J, Zhang J, Sun J. Numerical study of arc plasmas and weld pools for GTAW with applied axial magnetic fields. *Journal of Physics D: Applied Physics* 2012; 45(28): 285203.
- [23] Xu G, Hu J, Tsai HL. Three-dimensional modeling of the plasma arc in arc welding. *Journal of Applied Physics* 2008; 104(10): 103301.
- [24] Lin ZQ, Li YB, Wang YS, Chen GL. Numerical analysis of a moving gas tungsten arc weld pool with an external longitudinal magnetic field applied. *International Journal of Advanced Manufacturing Technology* 2005; 27(3-4): 288-295.
- [25] Blais A, Proulx P, Boulos MI. Three-dimensional numerical modelling of a magnetically deflected dc transferred arc in argon. *Journal of Physics D: Applied Physics* 2003; 36(5): 488-496.
- [26] Nomura K, Morisaki K, Hirata Y. Magnetic control of arc plasma and its modelling. *Welding in the World* 2009; 53: 181-187.

- [27] Nomura K, Ogino Y, Hirata Y. Shape control of TIG arc plasma by cusp-type magnetic field with permanent magnet. *Welding International* 2012; 26(10): 759-764.